Dalton Transactions

PAPER

View Article Online
View Journal | View Issue

Cite this: *Dalton Trans.*, 2015, **44**, 19200

Tin(II)-functionalization of the archetypal $\{P_8W_{48}\}$ polyoxotungstate†

N. V. Izarova,*[a] L. Klaß,[a,b] P. de Oliveira,[c] I.-M. Mbomekalle,[c] V. Peters,[b] F. Haarmann[b] and P. Kögerler*[a,b]

Received 16th August 2015,
Accepted 1st October 2015

DOI: 10.1039/c5dt03164h

www.rsc.org/dalton

The synthesis of $[K_{4.5} \subset (ClSn^{II})_8P_8W_{48}O_{184}]^{17.5-}$, featuring Sn(II) ions in trigonal-pyramidal SnO_2Cl environment coordinating to the two inner rims of the wheel-shaped $\{P_8W_{48}\}$-type polyoxotungstate(VI) archetype, showcases how high chloride ligand concentrations as well as the control of the polyanion solubility *via* electrolytes and evaporation rates are essential to prevent numerous competing reactions that can hamper the Sn(II) functionalization of polyoxometalates.

Introduction

The reactivity of main group metals towards polyoxotungstates (POTs) has received relatively little attention to date in comparison with that of transition metals and lanthanides. Among such main group metals, tin is one of the most investigated elements due to interest in POM functionalization with organotin moieties with Sn in its formal +IV oxidation state.[1] At the same time, examples of POTs incorporating Sn^{II} ions are still rather elusive, despite the general potential to exploit their structure-directing electron pair effect, in line with the lone pair effects that were *e.g.* utilized in the synthesis of As(III)-functionalized high-nuclearity POTs.[2]

In the pioneering work in the late 1970s, Knoth explored the possibility to attach organometallic $RMSn^{II}$ moieties (RM = $CpFe(CO)_2$, $(OC)_3Co$, π-C_3H_5Pd, $(C_7H_8)_2Rh$, *etc.*) to monolacunary Keggin-type POTs.[3a] Several years later, Chorghade and Pope thoroughly characterized a series of α/β-$[XW_{11}O_{39}Sn]^{n-}$ (X = B^{III}, Ga^{III}, Si^{IV}, Ge^{IV}, P^V) and α_2-$[P_2W_{17}O_{61}Sn]^{8-}$ complexes where Sn^{II} centers coordinate with monovacant Keggin- and Wells–Dawson-type species.[3b] A related polyanion with a postulated composition $[PMo_2W_9O_{39}Sn]^{5-}$ was reported to catalyze the oxidation of various organic sulfides to sulfoxides by H_2O_2.[3c]

In the complexes of Sn^{II} with α-A-isomers of trilacunary Keggin-type POTs two trivacant polyoxometalate (POM) ligands typically sandwich several tin(II) centers: three in $[Sn_3(XW_9O_{34})_2]^{n-}$ (X = Si^{IV}, P^V, As^V),[4] six in $[Sn_6(XW_9O_{33})_2]^{n-}$ (X = Sn^{II}, Sb^{III}),[5] or even nine in the polymeric $\{(H_2O)_mNa\}_n$-$[Cl_5Sn_9(XW_9O_{34})_2]_n$ (X = Si^{IV}, Ge^{IV}).[5b] In $[\{Sn_4(SiW_9O_{34})_2\}_2]^{24-}$ polyanions, which are catalytically active in hydrogen evolution from aqueous media, two $\{Sn_3(SiW_9O_{34})_2\}$ fragments are linked *via* two additional Sn^{II} centers into a dimer.[6] In the β-B-type trilacunary POTs $[Sn_{1.5}(WO_2(OH))_{0.5}(WO_2)_2(XW_9O_{33})_2]^{12-}$ (X = Sb^{III}, Bi^{III}) the Sn^{II} ions occupy the outer positions in the inner belt of the sandwich-type structure.[7] Sn^{II} ions in all the above mentioned species exhibit either trigonal or tetragonal pyramidal coordination environments and possess a lone electron pair, which, if sterically accessible, can be used for further functionalization of the Sn^{II}-containing POMs *via* coordination with organometallic moieties.

Besides acting as an external heterometal, Sn^{II} ions can also assume the role of internal heteroatoms composing POT structures as was observed in $[H_3SnW_{18}O_{60}]^{7-}$ (ref. 7) and the $\{SnW_9O_{33}\}$ subunit in the above-mentioned $[Sn_6(SnW_9O_{33})_2]^{8-}$,[5a] as well as act as a linker between the intact paratungstate-B structures leading to anionic chains $[\{H_2SnW_{12}O_{42}\}_n]^{8n-}$.[8]

At the same time the reactivity of Sn^{II} towards multilacunary (*i.e.* more reactive) derivatives of Wells–Dawson-type POTs or POMs with more complex structures remains unstudied. Therefore we decided to investigate the reaction of Sn^{II} chloride with the archetypal macrocyclic phosphotungstate $[P_8W_{48}O_{184}]^{40-}$ (= $\{P_8W_{48}\}$), possessing a wheel-shaped structure composed of four identical hexalacunary $\{P_2W_{12}O_{48}\}$ Wells–Dawson fragments connected to each other *via* oxo-bridges. The large inner cavity of $\{P_8W_{48}\}$ allows for the incorporation of a wide range of hetero-transition metal ions, as exemplified by $[Cu_{20}X(OH)_{24}(H_2O)_{12}P_8W_{48}O_{184}]^{25-}$ (X = Cl, Br, I),[9a,b] $[Cu_{20}(N_3)_6(OH)_{18}P_8W_{48}O_{184}]^{24-}$,[9c] $[K_8 \subset \{P_8W_{48}O_{184}\}\text{-}\{V^V_4V^{IV}_2O_{12}\text{-}$

[a]*Jülich-Aachen Research Alliance (JARA-FIT) and Peter Grünberg Institute – PGI 6, Forschungszentrum Jülich, D-52425 Jülich, Germany. E-mail: n.izarova@fz-juelich.de, paul.koegerler@ac.rwth-aachen.de*
[b]*Institute of Inorganic Chemistry, RWTH Aachen University, D-52074 Aachen, Germany*
[c]*Equipe d'Electrochimie et de Photoélectrochimie, Laboratoire de Chimie-Physique, Université Paris-Sud, UMR 8000 CNRS, Orsay F-91405, France*

† Electronic supplementary information (ESI) available: Crystallographic data in CIF format, BVS calculation details, crystal packing in **KLi-1**, IR/Raman, solid-state and time-dependent solution ^{31}P NMR and UV-vis spectra; TGA, CV and EQCM curves. See DOI: 10.1039/c5dt03164h

$(H_2O)_2\}_2]^{24-}$,[10a] $[Fe_{16}(OH)_{28}(H_2O)_4P_8W_{48}O_{184}]^{20-}$,[10b] $[K_8 \subset \{P_8W_{48}O_{184}\}\text{-}\{Mo^{VI}O_2\}_4\{Mo^{V}_4O_{10}(H_2O)_3\}_2]^{24-}$,[10c] and others.[11] $\{P_8W_{48}\}$ can also assume the role of a secondary building block in the carbon-free 3D coordination framework $K_{18}Li_6[Mn_8(H_2O)_{48}\text{-}P_8W_{48}O_{184}]\cdot 108H_2O$, exhibiting rigid cages with an approximate volume of 7.24 nm^3.[12]

Herein we report the first example of a $\{P_8W_{48}\}$ POT incorporating the main group element, namely the polyanion $[K_{4.5} \subset (ClSn^{II})_8P_8W_{48}O_{184}]^{17.5-}$ (**1**) that was synthesized in a one-pot reaction in an aqueous medium, isolated as the hydrated potassium/lithium salt $K_{10}Li_{17.5}[K_{4.5}\subset(ClSn^{II})_8\text{-}P_8W_{48}O_{184}]\cdot 50H_2O$ (**KLi-1**), and characterized by single-crystal X-ray, elemental and thermogravimetric analyses; FT-IR/Raman, UV-Vis, solid-state MAS and solution ^{31}P NMR spectroscopy as well as cyclic voltammetry and electrochemical quartz crystal microbalance studies.

Results and discussion

Synthesis

The polyanions **1** have been synthesized by the reaction of $[H_7P_8W_{48}O_{184}]^{33-}$ with $SnCl_2$ in 4 M aqueous LiCl solution at 50 °C. Alternatively heating at 50 °C for 1 h, the reaction mixture could be stirred at room temperature for 4–5 h. The large bright-orange block-shaped crystals of **KLi-1** form within several days by the evaporation of the obtained solutions under a hood. During the reaction the color of the reaction mixture changes from bright-orange to brown and then to dark-green indicating partial reduction of W^{VI} centers of $\{P_8W_{48}\}$ by Sn^{II} to W^{V} ions which are then slowly reoxidized by air oxygen. To minimize this undesirable process, lowering the yield of the product, a large excess of Sn^{II} ions should be excluded and access of the reaction mixture to air oxygen needs to be provided which is in part achieved by a sufficient surface/volume ratio of the reaction solution (that, in turn, makes difficult upscaling of the reaction volume). Prolonged heating of the reaction mixture as well as heating at higher temperatures (70–90 °C) speed up the W^{VI} reduction process and thus should be prevented. The evaporation rate of the reaction solution also seems to play a crucial role. Thus, evaporation under a fumehood results in the rapid crystallization of **KLi-1** within 1–6 days, while slower evaporation of the reaction mixture (*e.g.* outside a fumehood) leads to gradual decomposition of **1** with the formation of a white viscous gel-like precipitate. This product most likely represents a mixed Sn(II) chloride-hydroxide (Sn(OH)Cl), the formation of which is followed by a visible color change of the reaction mixture, which complicates the isolation of pure **KLi-1**. A relatively high Cl^- concentration is also important as it serves as a source of terminal chloride ligands on the Sn^{II} centers in **1**. Thus, the polyanion **1** cannot be crystallized from other media (*e.g.*, LiOAc (pH 2–6), NaOAc (pH 2–6), Li_2SO_4 (pH 2–3) or 2 M LiCl and NaCl) where the reaction products of $[H_7P_8W_{48}O_{184}]^{33-}$ with $SnCl_2$ turn out to be mixtures of hydrated K^+/Li^+ salts of polyanions with the general composition $[(HOSn^{II})_xP_8W_{48}O_{184}]^{(40-x)-}$ with x = 3–6. Representative examples which we were able to structurally characterize are $K_{46.75}Li_{26.25}[(HOSn^{II})_4P_8W_{48}O_{184}][(HOSn^{II})_3\text{-}P_8W_{48}O_{184}]\cdot nH_2O$ (CSD-430081) and $K_{11}Li_{23}[(HOSn^{II})_6P_8W_{48}O_{184}]\cdot nH_2O$ (CSD-430082), both of which exhibit correspondingly decreased crystallographic occupancy factors for the Sn positions.

Crystal structure analysis

Compound **KLi-1** crystallizes in tetragonal symmetry in the space group $I4/m$. The polyanion **1** consists of a macrocyclic phosphotungstate $\{P_8W_{48}\}$ which is coordinated by eight Sn^{II} ions that are located in the inner cavity of $\{P_8W_{48}\}$ at the eight vacant sites between neighboring $\{P_2W_{12}\}$ subunits. Each Sn center binds to two terminal oxygen positions belonging to two adjacent $\{P_2W_{12}\}$ groups (Sn–O 2.140(10)–2.152(11) Å; Fig. 1). Thus, the POM possesses an idealized D_{4h} symmetry. The bond lengths and angles within the phosphotungstate framework are in the usual range (see Table S1†).

Each Sn^{II} center resides in a trigonal pyramidal SnO_2Cl coordination environment with a terminal chloride ligand (Sn–Cl 2.515(6) Å) directed towards the center of the $\{P_8W_{48}\}$ ring. This trigonal-pyramidal coordination mode is reminiscent of several other anionic Sn(II) complexes such as $SnCl_3^-$, that are formed in aqueous solutions at higher halide concentrations, or $SnCl_2(H_2O)$. The Sn–Cl bond lengths in **1** can be compared with those of 2.523 and 2.595 Å in $Cs[SnCl_3]$[13a] and $[SnCl_2(H_2O)]\cdot H_2O$,[13b] respectively. The Sn–O bond distances in **1** also correlate rather well with the Sn–O bond lengths in $[SnCl_2(H_2O)]\cdot H_2O$ (2.169 Å)[13b] and other Sn^{II}-containing POTs.[3–8] The O–Sn–O and O–Sn–Cl angles are in the usual

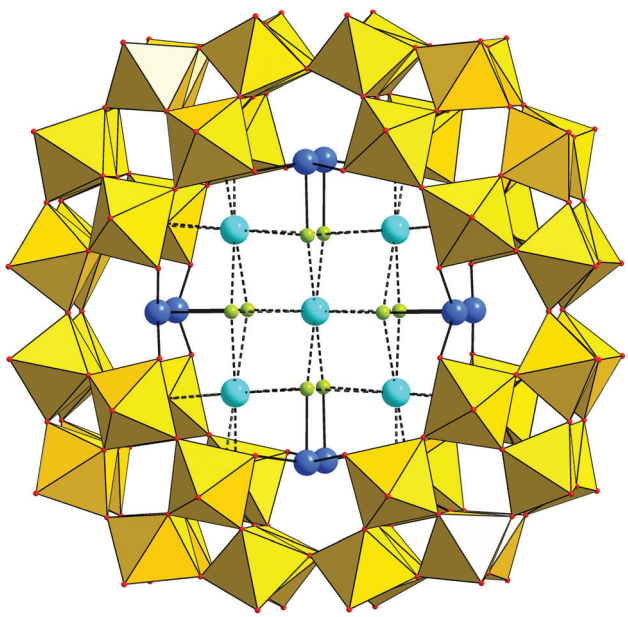

Fig. 1 Structure of **1** in combined polyhedral/ball-and-stick representation. Color legend: WO_6, yellow octahedra; Sn, blue; K, light blue; Cl, lime green; O, red spheres. The P centers are not visible in this perspective.

range and constitute 91.5(4)° and 85.8(3)–86.3(3)°, respectively. The lone electron pair on each Sn^{II} center is oriented towards the center of the polyanion and thus is sterically inaccessible. The closest Sn···Sn distances are 3.956(1) Å between the Sn^{II} centers situated on the opposite side of $\{P_8W_{48}\}$ and 7.248(1) Å between the Sn^{II} centers located on the same side of the wheel.

The inner cavity of **1** is occupied by four K^+ countercations each forming weak electrostatic interactions with four oxygen atoms of two phosphate groups of one of the $\{P_2W_{12}\}$ units (K–O: 2.815(11)–2.828(11) Å) and four chloride ligands on the adjacent Sn^{II} centers (K–Cl: 3.278(8)–3.301(8) Å). In addition, half of the polyanions in the solid-state structure of **KLi-1** incorporate a central K^+ cation, which coordinates eight Cl^- ligands of eight Sn^{II} ions (K–Cl: 3.155(5) Å).

According to bond valence sum calculations,[14] all tungsten centers in **1** are in the oxidation state +VI and all oxygen atoms of $\{P_8W_{48}\}$ are unprotonated (see Table S2†). Thus, the partial reduction of W^{VI} centers in the $\{P_8W_{48}\}$ precursor due to the reaction with Sn^{II} might explain the relatively low yield of **KLi-1**, the final formula of which was determined from crystal structural data, BVS calculations and elemental analysis.

To the best of our knowledge **1** is the first example of a $\{P_8W_{48}\}$-type polyanion with a main group metal, as only transition metal and lanthanide-functionalized $\{P_8W_{48}\}$ derivatives have been reported to date. The main difference in Sn^{II} (*vs.* transition metal/lanthanide) complexation with $\{P_8W_{48}\}$ is the relatively small coordination number (3) of Sn^{II}. This feature, however, limits the long-term solution stability of **1** (*vide infra*). On the other hand, it leaves rather a significant space inside the $\{Sn_8P_8W_{48}\}$ macrocycles that can potentially be used to incorporate other ligands/metals.

In the solid-state structure of **KLi-1** the polyanions **1** are interlinked *via* K^+ countercations into a 3D framework with pseudolayers of **1** packed in an ···ABABAB··· pattern (Fig. S1 and S2†) along the crystallographic *c* axis. A network of channels along the *a* and *b* axes with 5 × 9 Å diameter are filled by crystal water molecules.

FT-IR spectrum

The FT-IR spectrum of **KLi-1** (Fig. S3†) exhibits a set of bands in the range of 1135–400 cm^{-1} typical of the $\{P_8W_{48}\}$ framework. Thus, the positions of the bands characteristic of vibrations of P–O bonds in **KLi-1** (1134, 1084 and 1022 cm^{-1}) are almost the same as those attributed to P–O vibrations of a tin-free K/Li salt, **KLi-P_8W_{48}** (1138, 1085 and 1017 cm^{-1}), despite a small shoulder at 1120 cm^{-1} for **KLi-1**. The intense band at 926 cm^{-1} belongs to the stretching vibrations of the terminal W═O bonds. The main differences between **KLi-1** and **KLi-P_8W_{48}** in the 850–400 cm^{-1} range concern W–O–W, W–O–P and W–O–Sn vibrations (716, 569, 530, 465 and 401 cm^{-1} for **KLi-1** and 807, 686, 573, 527 and 472 cm^{-1} for **KLi-P_8W_{48}**) and, especially in the 850–550 cm^{-1} region, reflect the Sn^{II} coordination to $\{P_8W_{48}\}$.

Characterization in aqueous solution

KLi-1 is soluble in water, and its solubility is significantly enhanced in the presence of Li^+ ions. The addition of K^+ salts to solutions of **KLi-1** leads to immediate precipitation of the complex. The stability of the polyanions **1** in various Li^+-based media has been investigated by ^{31}P NMR and UV-Vis spectroscopy.

^{31}P NMR spectroscopy. The room temperature liquid-state ^{31}P NMR spectrum of **1** in a 2 M Li_2SO_4/H_2SO_4 buffer with pH 3.0 (Fig. 2) recorded within 1 h exhibits a single signal at −8.0 ppm which is in full agreement with the D_{4h} symmetry of **1** in the crystal lattice of **KLi-1**. It corresponds rather well to the signal at −7.6 ppm observed in the ^{31}P MAS NMR solid-state spectrum of **KLi-1** recorded at 67 kHz rotation frequency (Fig. S6†). Furthermore, it documents the single phase character of the material. The symmetric line shape of the ^{31}P NMR spectrum measured without sample spinning indicates the absence of a significant chemical shift anisotropy confirming the tetrahedral coordination of the phosphorus atoms. The small difference in the chemical shift can be attributed to the heating of the sample during its fast rotation in the solid-state measurements. This also can be compared with a singlet at −6.5 ppm characteristic of non-coordinated **KLi-P_8W_{48}** [15] measured in the same medium (Fig. S7†). This result indicates short-term stability of the title compound in 2 M Li_2SO_4/H_2SO_4 buffer (pH 3.0). At the same time, after several hours other signals start to appear in the spectrum evident of slow decomposition of **1** in aqueous solution *via* the gradual release of Sn^{II} ions. Thus, the spectrum of the same solution measured for 1 day (Fig. S8†) shows a set of additional, weaker signals at −8.1 ppm (13.6% of the total intensity of all the signals), −8.3 ppm (6.1%), −8.4 ppm (2.7%), −8.7 ppm (2.3%), −8.8 ppm (1.4%) and −10.7 ppm (6.4%) along with the original one at −8.0 ppm (67.5%). The decomposition of the polyanion in 4 M LiCl seems to be even faster, already after one hour the spectrum of **KLi-1** redissolved in this medium exhibits a set of badly resolved signals in the range of −6.3 to

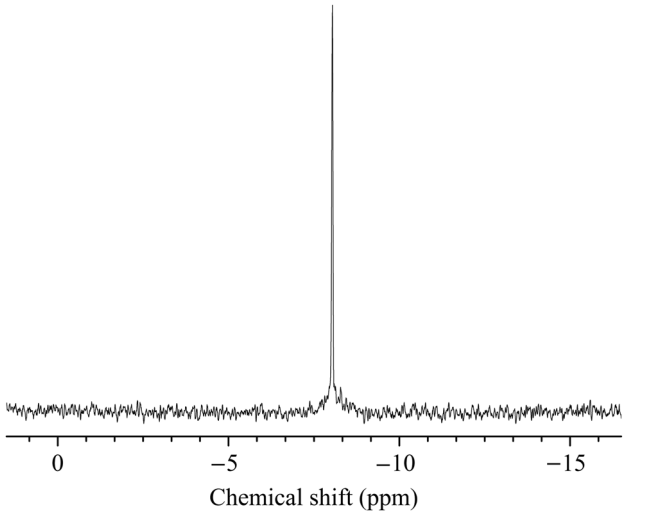

Fig. 2 Room temperature liquid-state ^{31}P NMR spectrum of **1** in 2 M Li_2SO_4/H_2SO_4 buffer solution (pH 3.0) after 1 h.

−7.5 ppm (85%) and two singlets at −8.0 (8.8%) and −10.7 ppm (6.2%). The ^{31}P NMR spectrum of **1** in this medium (Fig. S9†) does not change further significantly within 24 h. The signals at −8.1 and −10.7 ppm in the spectra measured in both 2 M Li_2SO_4 (pH 3.0) and 4 M LiCl after 24 h suggest the existence of a rather stable decomposition intermediate(s) of the $\{Sn_8P_8W_{48}\}$ complex, most likely of composition $\{Sn_xP_8W_{48}\}$ with $x < 8$, which form *via* the release of one or more Sn^{II} centers from $\{Sn_8P_8W_{48}\}$.

UV-Vis spectroscopy. The solutions of **KLi-1** were further examined using absorption spectroscopy to check for the solution stability of the $\{Sn_8P_8W_{48}\}$ complex at small concentrations (*ca.* 10^{-4} M). The UV-Vis spectrum of **KLi-1** redissolved in 2 M Li_2SO_4/H_2SO_4 buffer (pH 3.0) exhibits two strong absorption maxima at 216 nm (ε = 97 800 M^{-1} cm^{-1}) and 275 nm (ε = 97 800 M^{-1} cm^{-1}) and at 385 nm (ε = 9800 M^{-1} cm^{-1}), responsible for the orange color of the compound (Fig. S10†). Time-dependent measurements on solutions of **KLi-1** in 2 M Li_2SO_4/H_2SO_4 buffer (pH 3.0) ($c = 1.0 \times 10^{-4}$ M) show a gradual decrease in the intensity of the maximum at 385 nm starting after 1.5–2 h (Fig. S11 and S12†), which supports the conclusions on slow solution decomposition of the polyanions based on the ^{31}P NMR spectroscopy data. The spectra in some other media show similar characteristics (see the Experimental section and Fig. S13 and S14†).

Electrochemical studies. Compound **1** was studied by cyclic voltammetry in three different media: (1) 1 M LiCl + HCl (pH = 2.0); (2) 0.5 M Li_2SO_4 + H_2SO_4 (pH 2.0) and (3) 2 M LiCl (unbuffered). As expected, the medium in which the observed waves are best defined is the one exhibiting the highest buffering power, 0.5 M Li_2SO_4/H_2SO_4 (pH 2.0) (Fig. S15†). In fact, previous studies showed that the parent compound of **1**, the polyanion $\{P_8W_{48}\}$, reacts as an effective proton sponge.[16] The presence of 8 Sn^{II} centers does not seem to modify nor attenuate this behavior. A comparison of the CVs of **1** and $\{P_8W_{48}\}$ taken as reference, recorded in 0.5 M Li_2SO_4 + H_2SO_4 (pH 2.0) (Fig. 3), reveals three main differences: (I) the redox waves attributed to the W^{VI} centers are better separated on the CV of **1**, having two clearly defined reduction steps. (II) The reduction of the W^{VI} centers takes place at far less negative potentials compared to those of $\{P_8W_{48}\}$ (ΔV = 160 mV). (III) There is a new redox wave after those assigned to the reduction of the W^{VI} centers. This wave, with a shape characteristic of adsorption/desorption processes taking place on the surface of the working electrode, is assigned to the reduction of the Sn^{II} centers to Sn^0 and to the formation of a metallic tin film on the surface of the GC electrode. Upon scan reversal, there is the re-dissolution wave of tin concomitant with its electrochemical re-oxidation: $Sn^0 = Sn^{2+} + 2e^-$. When lower scan rates are employed and the potential is restricted to a range excluding this third wave ($E > -0.58$ V *vs.* SCE), it is clear that just the W^{VI} centers are reduced, and the Sn^{II} centers are not affected (Fig. S16†).

In order to prove unambiguously that the potential scan restricted to a range not going below −0.58 V *vs.* SCE concerns just the W centers, we carried out a study of the dependence of the reduction and oxidation peak currents, I_{pc} and I_{pa}, on the scan rate. It revealed that I_p depends on the square root of the scan rate, despite the fact that a relatively narrow set of scan rates was used (10 to 50 mV s^{-1}), this confirms that the mass transport phenomena coupled to the electron transfer are diffusion controlled, excluding the possible involvement of the Sn centers (Fig. S17†).

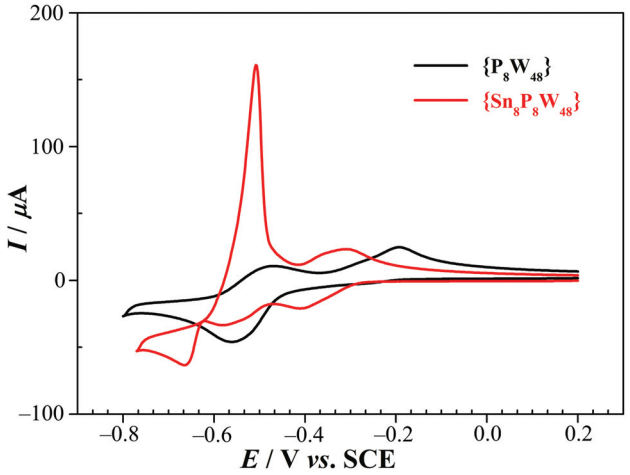

Fig. 3 CVs of **1** (red) and $\{P_8W_{48}\}$ (black) in 0.5 M Li_2SO_4 + H_2SO_4 (pH 2.0). POM concentration: 0.5 mM. Scan rate: 100 mV s^{-1}; working electrode: glassy carbon; reference electrode: SCE.

Electrochemical quartz crystal microbalance (EQCM) characterization. In order to confirm undoubtedly that there is a metal tin film forming on the surface of the working electrode during the cyclic voltammetry experiment when the potential range goes beyond the W centers' redox waves, meaning that a wave assignable to the $Sn^{II/0}$ redox couple is reached, a quartz crystal microbalance was coupled to the electrochemistry setup. A potential scan was carried out at a low rate (2 mV s^{-1}) in order to favor the deposit of the Sn^0 film. In addition, when two consecutive scans are recorded, the GC electrode surface is perfectly regenerated upon the reverse scan. The quartz crystal vibration frequency variation indicates that the Sn^0 film starts depositing at a potential of −0.6 V *vs.* SCE and continues even after the potential scan is reversed. This potential of −0.6 V *vs.* SCE seems to be the threshold value both for the onset of the Sn^{II} reduction and for the onset of the re-oxidation of Sn^0 (Fig. 4). It is possible to estimate the amount of accumulated tin after each cycle, but we did not find it crucial in the context of the present study.

Experimental section

General methods and materials

The reagents were used as purchased without further purification. $K_{28}Li_5[H_7P_8W_{48}O_{184}]\cdot 92H_2O$ (**KLi-P_8W_{48}**) was obtained according to the reported procedure[15] and its identity and purity were confirmed by IR and ^{31}P NMR spectroscopy.

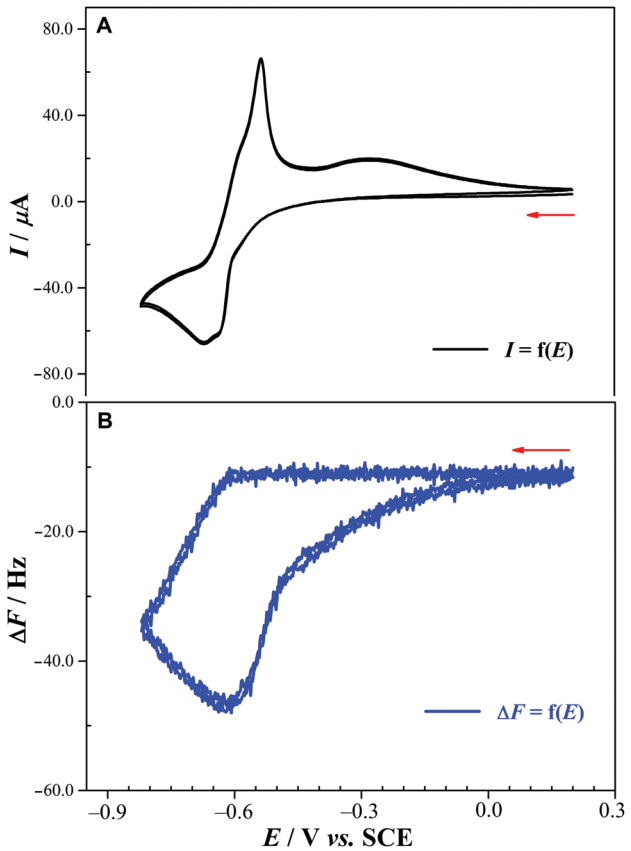

Fig. 4 (A) CV of **1** in 0.5 M Li_2SO_4 + H_2SO_4 (pH 2.0). Working electrode: glassy carbon-covered quartz crystal. Reference electrode: SCE. Scan rate: 2 mV s^{-1}. POM concentration: 0.5 mM. Potential scan extended to the reduction waves of the Sn^{II} centers. (B) Quartz crystal vibration frequency variation, ΔF, as a function of the working electrode potential.

Elemental analysis results (ICP-OES) were obtained from Central Institute for Engineering, Electronics and Analytics (ZEA-3), Forschungszentrum Jülich GmbH (D-52425 Jülich, Germany). TGA/DTA measurements were carried out with a Mettler Toledo TGA/SDTA 851 in dry N_2 (60 ml min^{-1}) at a heating rate of 5 K min^{-1}. Vibrational spectra were recorded on a Bruker Vertex 70 FT-IR spectrometer coupled with a RAM II FT-Raman module (1064 nm Nd:YAG laser) on KBr disks for the FT-IR and the solid material for the Raman measurements. UV-Vis spectra were recorded using 10 mm quartz cuvettes on an Analytik Jena Specord S600 spectrophotometer. Solution ^{31}P NMR spectra were recorded at room temperature in 5 mm tubes using a Bruker Avance 600 MHz spectrometer equipped with a prodigy probe, operating at 242.95 MHz for ^{31}P. Chemical shifts are reported with respect to 85% H_3PO_4; all chemical shifts downfield of the reference are reported as positive values. The solid-state ^{31}P NMR measurements were performed at ambient temperature using a Bruker Avance III spectrometer with a 9.4 T magnetic field. The spectrometer was equipped with a Bruker triple resonance probe for rotors of 1.3 mm diameter. The ground sample powder was filled into a ZrO_2 rotor for the experiments with and without sample spinning. A rotation frequency of 67 kHz was applied during MAS. An eight-fold cyclisation of the pulse sequences with a cycle delay of 10 s was used. The signal shift is referred to H_3PO_4.

Synthesis of $K_{10}Li_{17.5}[K_{4.5}\subset(ClSn)_8P_8W_{48}O_{184}]\cdot 50H_2O$ (KLi-1)

$K_{28}Li_5[H_7P_8W_{48}O_{184}]\cdot 92H_2O$ (0.10 g; 6.75 μmol) and $SnCl_2\cdot 2H_2O$ (0.013 g; 57.6 μmol) were dissolved in 3 mL of 4 M aqueous solution of LiCl in a 20 mL vial which was then closed with a screw cap. The reaction mixture was stirred at 50 °C for 1 h. During the heating the color of the solution was gradually changing from bright orange (obtained directly after the reagent dissolution) to brown and then to dark-green (originating from partial W^{VI} reduction). After that the reaction mixture was cooled down to room temperature and filtered. The obtained dark-green solution was then evaporated under a hood resulting in large block-shaped orange crystals of the product within 2 to 6 days. Yield: 0.025 g (25% based on $\{P_8W_{48}\}$).

Elemental analysis: calculated for $H_{100}Cl_8K_{14.5}Li_{17.5}O_{234}P_8Sn_8W_{48}$ (found): Cl, 1.91 (1.96); K, 3.82 (3.75); Li, 0.82 (0.83); P, 1.67 (1.45); Sn, 6.4 (6.1); W, 59.5 (61)%.

IR spectrum (KBr pellets), cm^{-1}: 3411 (s, br); 1620 (m); 1134 (m); 1120 (m); 1084 (m); 1022 (w); 926 (s); 716 (s); 569 (m); 530 (m); 465 (w); 401 (w).

Raman (solid sample, λ_e = 1064 nm), cm^{-1}: 1084 (w); 964 (s); 870 (w); 852 (w); 783 (m); 658 (m); 542 (w); 534 (w); 482 (w); 415 (w); 390 (w); 366 (w); 324 (w); 287 (w); 260 (m); 228 (m); 206 (m); 154 (m); 112 (m); 64 (s); 59 (s).

^{31}P NMR (H_2O/D_2O): −8.0 ppm (singlet). ^{31}P MAS NMR (67 kHz): −7.6 ppm (singlet).

UV-Vis (2 M Li_2SO_4 buffer solution, pH 3.0): λ = 216 nm, ε = 168 400 M^{-1} cm^{-1}; λ = 275 nm, ε = 97 800 M^{-1} cm^{-1}; λ = 385 nm, ε = 9789 M^{-1} cm^{-1}.

UV-Vis (0.5 M Li_2SO_4 buffer solution, pH 2.0): λ = 219 nm, ε = 214 600 M^{-1} cm^{-1}; λ = 274.5 nm, ε = 134 800 M^{-1} cm^{-1}; λ = 385 nm, ε = 8330 M^{-1} cm^{-1}.

X-ray crystallography

Single-crystal X-ray diffraction data for **KLi-1** were collected on a SuperNova (Agilent Technologies) diffractometer with Mo Kα radiation (λ = 0.71073 Å) at 120 K. A crystal was mounted on a Hampton cryoloop with Paratone-N oil to prevent water loss. Absorption corrections were applied numerically based on a multifaceted crystal model using CrysAlis software.[17] The SHELXTL software package[18] was used to solve and refine the structure. The structure was solved by the direct methods and refined by the full-matrix least-squares method against $|F|^2$ with anisotropic thermal parameters for all POM skeleton atoms (Sn, Cl, P, W, O) and potassium countercations and in isotropic approximation for the O atoms of co-crystallized solvent molecules. The Li^+ countercations and hydrogen atoms of the crystal water molecules were not located. The relative site occupancy factors for the disordered potassium countercations and solvent oxygens were first refined in an isotropic approximation with U_{iso} = 0.05 and then fixed at the

Table 1 Crystal data and structure refinement of KLi-1

Empirical formula	$H_{100}Cl_8K_{14.5}Li_{17.5}O_{234}P_8Sn_8W_{48}$
Formula weight, g mol^{-1}	14 838.88
Crystal system	Tetragonal
Space group	*I*4/*m*
a, Å	25.4151(3)
c, Å	21.7748(4)
Volume, Å^3	14 065.0(3)
Z	2
D_{calc}, g cm^{-3}	3.504
Absorption coefficient, mm^{-1}	20.666
F(000)	13 016
Crystal size, mm	0.19 × 0.28 × 0.35
Theta range for data collection	4.09°–26.02°
Completeness to Θ_{max}	99.4%
Index ranges	$-31 \le h \le 30$, $-31 \le k \le 30$, $-22 \le l \le 26$
Reflections collected	35 937
Independent reflections	7076
R_{int}	0.1192
Observed ($I > 2\sigma(I)$)	5862
Absorption correction	Empirical using spherical harmonics
T_{min}/T_{max}	0.0562/0.1109
Data/restraints/parameters	7076/36/379
Goodness-of-fit on F^2	1.092
R_1, wR_2 ($I > 2\sigma(I)$)	R_1 = 0.0583, wR_2 = 0.1563
R_1, wR_2 (all data)	R_1 = 0.0709, wR_2 = 0.1691
Largest diff. peak and hole, e Å^{-3}	6.755 and −3.837

obtained values and refined without the thermal parameter restrictions.

The number of crystal water molecules found by XRD was smaller than that determined by elemental analysis and TGA (41 *vs.* 50 and 102, respectively) reflecting the high degree of solvent disorder in the solid-state structure of **KLi-1**. This is also consistent with large solvent-accessible volume remaining in the structure. On the other hand, the sample used for TGA was dried to less than that taken for elemental analysis (2 days *vs*. 3 to 4 weeks). For the overall consistency the formula in the CIF file corresponds to the composition of the bulk material determined by elemental analysis since all the further studies were performed on the isolated well-dried bulk material of **KLi-1**.

Additional crystallographic data are summarized in Table 1. Further details on the crystal structure investigation may be obtained from Fachinformationszentrum Karlsruhe, 76344 Eggenstein-Leopoldshafen, Germany [fax (+49) 7247-808-666; e-mail crysdata@fiz-karlsruhe.de], upon quoting the depository number CSD 429908.

Electrochemical experiments

Cyclic voltammograms of **1** were recorded in comparison with the heterometal-free $\{P_8W_{48}\}$ salt **KLi-P$_8$W$_{48}$** at room temperature in three different media: (1) on a 0.55 mM solution of **KLi-1** in 1 M LiCl/HCl buffer (pH 2.0), (2) 0.57 mM solution of **KLi-1** in 0.5 M Li_2SO_4/H_2SO_4 buffer (pH 2.0) and (3) 0.52 mM non-buffered **KLi-1** solution in 2 M LiCl. The corresponding concentrations of **KLi-P$_8$W$_{48}$** were 0.51 mM, 0.56 mM and 0.53 mM, respectively. Electrochemical data were obtained using an EG&G 273A potentiostat controlled by M270 software. A conventional one-compartment three-electrode electrochemical cell included a glassy carbon working electrode (GC, Mersen, France) with a diameter of 3 mm, a platinum gauze counter electrode with a large surface area and a saturated calomel reference electrode. The source, mounting, and polishing of the glassy carbon electrode has been previously described.[19] The reference and counter electrodes were separated from the studied solutions *via* fritted compartments filled with the same electrolyte. Prior to the experiments the solutions were thoroughly deaerated with pure argon for at least 30 min and then kept under a positive argon pressure during the measurements. The midpoint redox potentials were determined from the average values of the anodic and cathodic peak potentials and are reported *vs.* the saturated calomel reference electrode (SCE).

The electrochemical quartz crystal microbalance (EQCM) measurements were carried out using a QCA 922 (Seiko/EG&G) system with 9 MHz AT-cut crystals. New crystals equipped with carbon electrodes possessing a true surface area of 0.3 cm^2 were provided by Seiko. Frequency variations were recorded and used for discussion in this work.

Conclusions

In summary, we have prepared the first complex of macrocyclic phosphotungstate with the main group metal ions, $[K_{4.5}\subset(ClSn)_8P_8W_{48}O_{184}]^{17.5-}$ (**1**), which also represents a rather rare example of Sn^{II}-containing POMs. In **1** the Sn^{II} centers occupy the eight vacant sites of the polyanion resulting in the POT with D_{4h} symmetry. Polyanions **1** have been isolated in the solid state as the hydrated mixed potassium/lithium salt **KLi-1** and characterized by single-crystal X-ray diffraction, FT-IR/Raman and ^{31}P MAS NMR spectroscopy as well as by elemental and thermogravimetric analyses. Solution studies by ^{31}P NMR, UV-Vis and electrochemistry showed that the complex is stable in aqueous medium for several hours and then slowly decomposes, releasing Sn^{II}. In contrast with transition metal and lanthanide-functionalized POMs, the Sn^{II} ions in **1** display a small coordination number of 3 and coordinate only one terminal Cl$^-$ ligand each, thus retaining a relatively large void in the inner cavity of the macrocyclic complex. Currently we are investigating the possibility of further functionalization of $\{Sn_8P_8W_{48}\}$ *via* incorporation of various heterometals in this inner core volume.

Acknowledgements

We gratefully acknowledge financial support by Forschungszentrum Jülich and the EU ERC Starting Grant MOLSPINTRON, no. 308051 (P.K.) as well as by the Université Paris-Sud and the CNRS (I.M.M and P.d.O.) and by an STSM action

attributed by the COST CM1203 "Polyoxometalate Chemistry for Molecular Nanoscience (PoCheMoN)".

Notes and references

1 See for example: (*a*) P. Gouzerh and A. Proust, *Chem. Rev.*, 1998, **98**, 77–111; (*b*) A. Proust, R. Thouvenot and P. Gouzerh, *Chem. Commun.*, 2008, 1837–1852; (*c*) A. Dolbecq, E. Dumas, C. R. Mayer and P. Mialane, *Chem. Rev.*, 2010, **110**, 6009–6048; (*d*) M.-P. Santoni, G. S. Hanan and B. Hasenknopf, *Coord. Chem. Rev.*, 2014, **281**, 64–85, and references therein.

2 See for example: (*a*) S. Duval, M.-A. Pilette, J. Marrot, C. Simonnet-Jégat, M. N. Sokolov and E. Cadot, *Chem. – Eur. J.*, 2008, **14**, 3457–3466; (*b*) Y. Zhang, L. Li, T. Sun, B. Liu, H. Hu and G. Xue, *Inorg. Chem.*, 2011, **50**, 2613–2618; (*c*) C. Ritchie, M. Speldrich, R. W. Gable, L. Sorace, P. Kögerler and C. Boskovic, *Inorg. Chem.*, 2011, **50**, 7004–7014; (*d*) S. Duval, J. Marrot, C. Simonnet-Jégat, I. M. Mbomekalle, M. N. Sokolov and E. Cadot, *Dalton Trans.*, 2012, **41**, 3174–3184.

3 (*a*) W. H. Knoth, *J. Am. Chem. Soc.*, 1979, **101**, 2211–2213; (*b*) G. S. Chorghade and M. T. Pope, *J. Am. Chem. Soc.*, 1987, **109**, 5134–5138; (*c*) E. Rafiee, I. M. Baltork, S. Tangestaninejad, A. Azad and S. Moinee, *Z. Naturforsch., B: Chem. Sci.*, 2006, **61**, 601–606.

4 (*a*) F. Xin and M. T. Pope, *J. Am. Chem. Soc.*, 1996, **118**, 7731–7736; (*b*) A. Botar, B. Botar, P. Gili, A. Müller, J. Meyer, H. Bögge and M. Schmidtmann, *Z. Anorg. Allg. Chem.*, 1996, **622**, 1435–1440; (*c*) R. Khoshnavazi and L. Bahrami, *J. Coord. Chem.*, 2009, **62**, 2067–2075.

5 (*a*) M. N. Sokolov, N. V. Izarova, A. V. Virovets, V. P. Fedin, Z. A. Starikova and M. Yu. Antipin, *Dalton Trans.*, 2003, 4389–4390; (*b*) C. Zhao, E. N. Glass, B. Chica, D. G. Musaev, J. M. Sumliner, R. B. Dyer, T. Lian and C. L. Hill, *J. Am. Chem. Soc.*, 2014, **136**, 12085–12091.

6 Z. Zhang, Q. Lin, S.-T. Zheng, X. Bu and P. Feng, *Chem. Commun.*, 2011, **47**, 3918–3920.

7 B. Krebs, E. Droste, M. Piepenbrink and G. Vollmer, *C. R. Acad. Sci., Ser. IIc: Chim.*, 2000, **3**, 205–210.

8 M. N. Sokolov, I. V. Kalinina, E. V. Peresypkina, N. K. Moroz, D. Yu. Naumov and V. P. Fedin, *Eur. J. Inorg. Chem.*, 2013, 1772–1779.

9 (*a*) S. S. Mal and U. Kortz, *Angew. Chem., Int. Ed.*, 2005, **44**, 3777–3780; (*b*) S. S. Mal, B. S. Bassil, M. Ibrahim, S. Nellutla, J. van Tol, N. S. Dalal, J. A. Fernández, X. López, J. M. Poblet, R. Ngo Biboum, B. Keita and U. Kortz, *Inorg. Chem.*, 2009, **48**, 11636–11645; (*c*) C. Pichon, P. Mialane, A. Dolbecq, J. Marrot, E. Rivière, B. Keita, L. Nadjo and F. Sécheresse, *Inorg. Chem.*, 2007, **46**, 5292–5301.

10 (*a*) A. Müller, M. T. Pope, A. M. Todea, H. Bögge, J. van Slageren, M. Dressel, P. Gouzerh, R. Thouvenot, B. Tsukerblat and A. Bell, *Angew. Chem., Int. Ed.*, 2007, **46**, 4477–4480; (*b*) S. S. Mal, M. H. Dickman, U. Kortz, A. M. Todea, A. Merca, H. Bögge, T. Glaser, A. Müller, S. Nellutla, N. Kaur, J. van Tol, N. S. Dalal, B. Keita and L. Nadjo, *Chem. – Eur. J.*, 2008, **14**, 1186–1195; (*c*) F. L. Sousa, H. Bögge, A. Merca, P. Gouzerh, R. Thouvenot and A. Müller, *Chem. Commun.*, 2009, 7491–7493.

11 (*a*) M. Zimmermann, N. Belai, R. J. Butcher, M. T. Pope, E. V. Chubarova, M. H. Dickman and U. Kortz, *Inorg. Chem.*, 2007, **46**, 1737–1740; (*b*) S. S. Mal, N. H. Nsouli, M. H. Dickman and U. Kortz, *Dalton Trans.*, 2007, 2627–2630; (*c*) S. G. Mitchell, D. Gabb, C. Ritchie, N. Hazel, D.-L. Long and L. Cronin, *CrystEngComm*, 2009, **11**, 36–39; (*d*) B. S. Bassil, M. Ibrahim, S. S. Mal, A. Suchopar, R. Ngo Biboum, B. Keita, L. Nadjo, S. Nellutla, J. van Tol, N. S. Dalal and U. Kortz, *Inorg. Chem.*, 2010, **49**, 4949–4959; (*e*) S. G. Mitchell, T. Boyd, H. N. Miras, D.-L. Long and L. Cronin, *Inorg. Chem.*, 2011, **50**, 136–143; (*f*) X. Fang, P. Kögerler, Y. Furukawa, M. Speldrich and M. Luban, *Angew. Chem., Int. Ed.*, 2011, **50**, 5212–5216; (*g*) S.-W. Chen, K. Boubekeur, P. Gouzerh and A. Proust, *J. Mol. Struct.*, 2011, **994**, 104–108; (*h*) V. S. Korenev, S. Floquet, J. Marrot, M. Haouas, I.-M. Mbomekallé, F. Taulelle, M. N. Sokolov, V. P. Fedin and E. Cadot, *Inorg. Chem.*, 2012, **51**, 2349–2358; (*i*) Z.-J. Liu, Z.-M. Zhang, H. Fu, Y.-G. Li, W.-L. Chen, H.-H. Wu and E.-B. Wang, *Dalton Trans.*, 2012, **41**, 11700–11705; (*j*) L. Huang, L. Cheng, W.-H. Fang, S.-S. Wang and G.-Y. Yang, *Eur. J. Inorg. Chem.*, 2013, 1693–1698; (*k*) Y.-Q. Jiao, C. Qin, X.-L. Wang, C.-G. Wang, C.-Y. Sun, H.-N. Wang, K.-Z. Shao and Z.-M. Su, *Chem. – Asian J.*, 2014, **9**, 470–478.

12 S. G. Mitchell, C. Streb, H. N. Miras, T. Boyd, D. L. Long and L. Cronin, *Nat. Chem.*, 2010, **2**, 308–312.

13 (*a*) F. R. Poulsen and S. E. Rasmussen, *Acta Chem., Scand.*, 1970, **24**, 150–156; (*b*) B. Kamenar and D. Grdenic, *J. Chem. Soc.*, 1961, 3954–3958.

14 (*a*) I. D. Brown and D. Altermatt, *Acta Crystallogr., Sect. B: Struct. Sci.*, 1985, **41**, 244–247; (*b*) K. Knížek, Kalvados – Software for crystal structure and powder diffraction; see http://www.fzu.cz/~knizek/kalvados/index.html.

15 R. Contant and A. Tézé, *Inorg. Chem.*, 1985, **24**, 4610–4614.

16 B. Keita, Y. W. Lu, L. Nadjo and R. Contant, *Electrochem. Commun.*, 2000, **2**, 720–726.

17 *CrysAlisPro, Version 1.171.36.21 (release 14-08-2012 CrysAlis171.NET)*, Agilent Technologies.

18 G. M. Sheldrick, *Acta Crystallogr., Sect. A: Fundam. Crystallogr.*, 2008, **64**, 112–122.

19 N. Vila, P. A. Aparicio, F. Sécheresse, J. M. Poblet, X. Lopez and I. M. Mbomekallé, *Inorg. Chem.*, 2012, **51**, 6129–6138.

